Modeling the coupled effects of pore space geometry and velocity on colloid transport and retention

Scott A. Bradford,[1] Saeed Torkzaban,[2] Feike Leij,[3] Jiri Šimůnek,[2] and Martinus T. van Genuchten[4]

Received 16 April 2008; revised 31 October 2008; accepted 2 December 2008; published 12 February 2009.

[1] Recent experimental and theoretical work has demonstrated that pore space geometry and hydrodynamics can play an important role in colloid retention under unfavorable attachment conditions. Conceptual models that only consider the average pore water velocity and a single attachment rate coefficient are therefore not always adequate to describe colloid retention processes, which frequently produce nonexponential profiles of retained colloids with distance. In this work, we highlight a dual-permeability model formulation that can be used to account for enhanced colloid retention in low-velocity regions of the pore space. The model accounts for different rates of advective and dispersive transport, as well as first-order colloid retention and release in fast and slow velocity regions of the pore space. The model also includes provisions for the exchange of colloids from fast to slow regions in the aqueous phase and/or on the solid phase. A sensitivity analysis performed with the dual-permeability model parameters indicated that low rates of advective transport to low-velocity regions had a pronounced influence on colloid retention profiles, especially near the inlet. The developed model provided a good description of measured colloid breakthrough curves and retention profiles that were collected for a variety of conditions.

Citation: Bradford, S. A., S. Torkzaban, F. Leij, J. Šimůnek, and M. T. van Genuchten (2009), Modeling the coupled effects of pore space geometry and velocity on colloid transport and retention, *Water Resour. Res.*, *45*, W02414, doi:10.1029/2008WR007096.

1. Introduction

[2] Accurate simulations of the transport and retention of colloids in porous media is needed for a wide variety of applications: to protect water supplies from pathogenic microorganisms [*Gerba et al.*, 1996; *Loge et al.*, 2002; *Abbaszadegan et al.*, 2003] and a variety of colloid associated contaminants [*Grolimund et al.*, 1996; *Kim et al.*, 2003; *Chen et al.*, 2005; *Šimůnek et al.*, 2006]; to quantify processes of soil genesis, erosion, and aquifer and petroleum reservoir production [*Khilar and Fogler*, 1998; *Mays and Hunt*, 2005]; and to improve engineered bioremediation strategies [*Mishra et al.*, 2001; *Vidali*, 2001]. Most models for colloid migration in porous media consider only the average pore water velocity in the porous medium and a single attachment rate coefficient to quantify interactions between the colloids and the solid surfaces [*Yao et al.*, 1971; *Rajagopalan and Tien*, 1976]. These models predict that colloids move with the average pore water velocity and that the profile of retained colloids in porous media will decrease exponentially with distance. Filtration theory [*Yao et al.*, 1971] is commonly used in such models to predict the attachment rate coefficient. In this case, the rate of mass transfer of colloids to solid surfaces by sedimentation, interception, and diffusion is quantified from correlation expressions [*Logan et al.*, 1995; *Tufenkji and Elimelech*, 2004; *Nelson and Ginn*, 2005] that were determined from single collector simulation results using the sphere-in-cell model. Interactions of colloids with the solid surface are subsequently assumed to be controlled by physicochemical forces that can be quantified using a theory developed by Derjaguin, Landau, Verwey, and Overbeek (DLVO) [*Derjaguin and Landau*, 1941; *Verwey and Overbeek*, 1948].

[3] Filtration theory has proven to be a useful tool for predicting colloid transport and retention in porous media under conditions that are favorable for attachment [*Yao et al.*, 1971; *Rajagopalan and Tien*, 1976; *Harvey and Garabedian*, 1991; *Li and Johnson*, 2005], for example when there is no energy barrier to attachment of colloids in the primary minimum of the DLVO interaction energy profile. Conversely under unfavorable attachment conditions (when there is an energy barrier to attachment in the primary minimum), models that are based on filtration theory have commonly been found inadequate to predict the amount of retention, the shape of the deposition profile, and the dependence of colloid retention on velocity, solution chemistry, and grain and colloid size [*Bradford et al.*, 2003, 2006, 2007; *Tufenkji and Elimelech*, 2005; *Tong et al.*, 2005; *Li and Johnson*, 2005; *Li et al.*, 2005; *Johnson et al.*, 2007a; *Torkzaban et al.*, 2007, 2008a, 2008b]. Variations in porous media and/or colloid surface charge have frequently been

[1] US Salinity Laboratory, ARS, USDA, Riverside, California, USA.
[2] Department of Environmental Science, University of California, Riverside, California, USA.
[3] Civil Engineering and Construction Engineering Management, California State University, Long Beach, California, USA.
[4] Department of Mechanical Engineering, Federal University of Rio de Janeiro, Rio de Janeiro, Brazil.

0043-1397/09/2008WR007096$09.00

invoked as a potential explanation for nonexponential deposition profiles, leading to the development of multiple deposition rate models to describe such behavior [*Grolimund and Borkovec*, 2001; *Tufenkji et al.*, 2003]. Furthermore, mobile colloids have sometimes been reported to be transported at a velocity that is higher than the average pore water velocity [*Cumbie and McKay*, 1999; *Ginn*, 2002].

[4] Filtration theory quantifies the rate of mass transfer of colloids to soil surfaces, and assumes that colloid retention is controlled by chemical interactions. In reality, colloid retention will depend on the forces and torques that act on colloids near solid surfaces [*Cushing and Lawler*, 1998; *Bergendahl and Grasso*, 2000; *Torkzaban et al.*, 2007]. The most significant forces that act on colloids near a solid surface are thought to be due to adhesion (chemical interactions), hydrodynamics, and diffusion [*Cushing and Lawler*, 1998; *Johnson et al.*, 2007b; *Bradford and Torkzaban*, 2008]. Under favorable attachment conditions adhesive forces will likely dominate colloid retention, as assumed by filtration theory [*Torkzaban et al.*, 2007]. Conversely, under unfavorable attachment conditions that are typical for most natural subsurface environments and colloids, the influence of hydrodynamics and diffusion cannot be neglected [*Cushing and Lawler*, 1998; *Simoni et al.*, 1998; *Bergendahl and Grasso*, 2000; *Dong et al.*, 2002; *Torkzaban et al.*, 2007]. Lifting, sliding, and rolling are hydrodynamic mechanisms that can cause colloid removal from an interface [*Hubbe*, 1984; *Soltani and Ahmadi*, 1994; *Bergendahl and Grasso*, 2000]. Rolling has been reported to be the dominant hydrodynamic mechanism of detachment from solid surfaces under laminar flow conditions [*Tsai et al.*, 1991; *Bergendahl and Grasso*, 1998, 1999].

[5] Colloids can interact with solid surfaces via the secondary minimum of the DLVO interaction energy profile under unfavorable attachment conditions [*Franchi and O'Melia*, 2003; *Redman et al.*, 2004; *Hahn and O'Melia*, 2004; *Hahn et al.*, 2004; *Tufenkji and Elimelech*, 2005]. In this case, consideration of the balance between adhesive (due to the secondary minimum) and hydrodynamic torques indicates that low-velocity regions may be hydrodynamically and chemically favorable for colloid retention [*Bradford et al.*, 2007; *Bradford and Torkzaban*, 2008; *Torkzaban et al.*, 2007, 2008a, 2008b]. During steady state fluid flow the hydrodynamic forces that occur near a single collector grain or in porous media are highly dependent on the spatial location along the solid surface. Specifically, lower-hydrodynamic forces occur on a single collector grain near the front and rear stagnation points, whereas in porous media lower velocities occur at grain-to-grain contacts, solid-air-water triple points, and in the smallest regions of the pore space [*Bradford et al.*, 2007; *Bradford and Torkzaban*, 2008; *Torkzaban et al.*, 2007, 2008b]. Indeed, recent experimental evidence by *Kuznar and Elimelech* [2007] demonstrated that colloids captured in the secondary energy minimum can be translated along the collector surface via hydrodynamic forces and be retained in regions near the rear stagnation point.

[6] The pore space geometry may cause fluid streamlines to separate from the grain surface, and to form low-velocity regions near the gaps between grains [*Davis et al.*, 1976; *Davis and O'Neill*, 1977; *Taneda*, 1979]. In these locations water does not mix with the bulk solution, but rather rotates in an infinite set of nested ring vortices. This type of behavior of Stokes flow around two spheres in contact or close to each other has theoretically been demonstrated [*Davis et al.*, 1976; *Davis and O'Neill*, 1977] and experimentally visualized by *Taneda* [1979]. The literature also indicates that pore-scale fluid flow is hydrodynamically disconnected from the bulk fluid flow (eddy zones) near solid-air-water triple points [*Sheng and Zhou*, 1992]. It should be mentioned that low-velocity regions in porous media have been used to explain a variety of observed transport behavior without recognizing the exact system hydrodynamics [*Padilla et al.*, 1999; *Toride et al.*, 2003]. *Torkzaban et al.* [2008b] recently demonstrated that these low-velocity regions can have a very significant effect on bacteria retention in saturated systems, and can retain bacteria in these locations even when the adhesive force is negligible.

[7] Fluorescent microscopy and X-ray microtomography studies have also demonstrated that colloids accumulate in narrow regions of pore spaces near the contacts of irregularly shaped sand grains under unfavorable attachment conditions [*Bradford et al.*, 2005, 2006; *Xu et al.*, 2006; *Li et al.*, 2006; *Yoon et al.*, 2006; *Gaillard et al.*, 2007]. In these studies, pore-space constrictions served as locations for colloid retention, whereas few colloids were immobilized far from the grain-to-grain contacts. Colloid retention in the smallest regions of the pore space, such as those formed near grain to grain contact points, has been referred to in the literature as straining [*Hill*, 1957; *McDowell-Boyer et al.*, 1986; *Cushing and Lawler*, 1998; *Bradford et al.*, 2006].

[8] The above literature indicates that, under unfavorable attachment conditions, colloid retention will primarily occur in the low-velocity regions of the porous media. It is therefore not surprising that models that consider only the average pore water velocity and a single attachment coefficient have been found to be inadequate to predict colloid retention behavior in many instances. The objective of this work is to present an alternative model formulation that can be used to account for different colloid retention mechanisms in the various regions of the pore space. Applications, implications, and limitations of this model to characterize colloid transport and retention will be demonstrated and discussed.

2. Pore-Scale Considerations

[9] Once colloids are transported to the solid surface in porous media, colloid retention under unfavorable attachment conditions will depend on a balance of forces and torques that act on colloids at this location [*Cushing and Lawler*, 1998; *Bergendahl and Grasso*, 2000; *Torkzaban et al.*, 2007]. Calculated locations on the solid surface that are chemically and hydrodynamically favorable for the retention of colloids may be determined from a balance of adhesive (T_{adhesive}; ML^2T^{-2}; where M, L, and T denote units of mass, length, and time, respectively) and hydrodynamic ($T_{\text{hydrodynamic}}$; ML^2T^{-2}) torques that act on colloids at the solid surface. Colloid retention only occurs on regions of the solid surface where $T_{\text{adhesive}} > T_{\text{hydrodynamic}}$. A detailed description to calculate T_{adhesive} and $T_{\text{hydrodynamic}}$ has recently been provided by *Torkzaban et al.* [2007, 2008b]. In brief, T_{adhesive} for colloids attached in the

secondary minimum of the DLVO interaction energy profile can be estimated using DLVO and Johnson, Kendall, and Roberts (JKR) theories [*Johnson et al.*, 1971; *Soltani and Ahmadi*, 1994; *Bergendahl and Grasso*, 2000; *Torkzaban et al.*, 2007; *Ahmadi et al.*, 2007], while $T_{\text{hydrodynamic}}$ may be determined using available theory in the literature [*Goldman et al.*, 1967; *O'Neill*, 1968; *Sharma et al.*, 1992].

[10] Application of the torque balance approach in natural porous media is limited by our knowledge of the exact pore-scale geometry and hydrodynamics, which influence both the rate of colloid mass transfer to solid surfaces and the hydrodynamic forces and torques acting on retained colloids. It is currently not computationally feasible to simulate all of the full three-dimensional pore-scale water flow and colloid transport processes at length-scales that are much greater than a few pores. Alternatively, simple geometries are sometimes used to provide insight about flow and transport processes that occur in natural porous media. In a capillary tube analogy of a porous medium the pore-scale velocity distribution is well known and the value of $T_{\text{hydrodynamic}}$ can be determined as [*Goldman et al.*, 1967; *O'Neill*, 1968; *Sharma et al.*, 1992; *Bergendahl and Grasso*, 2000]

$$T_{\text{hydrodynamic}} = 14.29\pi\mu r_c^3 \frac{\partial \text{v}}{\partial r} = 7.14\pi r_c^3 \frac{\Delta P}{L_{ct}}(R_c - r_c) \quad (1)$$

where μ [M $L^{-1}T^{-1}$] is the viscosity, r_c [L] is the colloid radius, R_c [L] is the capillary tube radius, r [L] is the radial direction from the solid surface, $\boldsymbol{v}$ [L T^{-1}] is the pore-scale velocity vector, and $\Delta P/L_{ct}$ [M L^{-2} T^{-2}] is the gradient in pressure over the capillary tube length. When $T_{\text{adhesive}} = T_{\text{hydrodynamic}}$ the value of R_c in equation (1) can be solved to determine a critical capillary tube radius for which colloid retention will occur in equal and smaller sized tubes as

$$R_c = \frac{\Gamma_{adhesive} L_{ct}}{7.14\pi r_c^3 \Delta P} + r_c \quad (2)$$

Alternatively, the value of R_c may also be estimated from a geometric analysis. *Herzig et al.* [1970] suggested that when several colloids arrive simultaneously at a pore then the value of R_c will become some multiple of the colloid radius.

[11] The volume fraction, γ [−], of pore space where colloid retention will occur can theoretically be determined from R_c and from measured capillary pressure curves and residual saturations. In this case, the capillary pressure curve is rewritten in terms of effective pore diameters using Laplace's equation by assuming that soil pores can be approximated as a bundle of cylindrical capillaries that are tortuous [e.g., *Dane and Hopmans*, 2002; *Flint and Flint*, 2002]. If a measured capillary pressure curve is parameterized using the model of *van Genuchten* [1980], then γ is given as

$$\gamma = (1 - S_{rw}) * \left[1 + \left(\frac{2\sigma\alpha_p}{\rho g R_c}\right)^n\right]^{-m} + S_{rw} \quad (3)$$

where S_{rw} [−] is residual water saturation, α_p[L^{-1}] is the reciprocal of the air entry pressure head, ρ [M L^{-3}] is the density of water, g [L T^{-2}] is the acceleration due to gravity, σ [M T^{-2}] is the surface tension, and m [−] and n [−] are fitting parameters. It should be mentioned that *Bradford et al.* [2006] used equation (3) and average measured capillary pressure-saturation parameters from various soil types to estimate values of γ. Depending on soil type from 10 to 71, 10 to 86, and 10 to 92% of the pore space was found to be smaller than 0.1, 2, and 6 μm colloids, respectively [*Bradford et al.*, 2006].

[12] Although the capillary tube analogy will undoubtedly have some significant limitations in describing the exact pore-scale geometry, the hydrodynamics, and the adhesive forces involved, equations (1)–(3) do provide useful insight on trends that can be expected for colloid retention in porous media. For example, equations (2) and (3) indicate that γ is expected to increase for increasing adhesive forces (T_{adhesive}) and to decrease for increasing flow rates (pressure gradient). This finding is consistent with recent pore-scale simulations of colloid retention on single collector surfaces [*Torkzaban et al.*, 2007]. Furthermore, the influence of pore space geometry and colloid size can be related to measurable relationships in equation (3).

3. Dual-Permeability Model

[13] At the column-scale the water flow and colloid transport parameters are averaged over a representative elementary volume (REV) to obtain effective parameters. Because of this averaging process some pore-scale flow and transport information is lost, such as the pore-scale distribution of the flow velocity and the exact location of colloid retention. The implicit assumption of this averaging procedure is that the lost pore-scale information does not control the flow and transport processes. The literature review and the information presented above indicate that this assumption may be violated for colloid transport and retention in porous media under unfavorable attachment conditions. Below we present a REV scale model to better account for the observed pore-scale physics that was discussed above.

[14] Dual-permeability models have commonly been used to study preferential and nonequilibrium flow and solute transport in structured soils and fractured rocks [*Šimůnek et al.*, 2003; *Gerke*, 2006; *Šimůnek and van Genuchten*, 2008]. In this case, the dual-permeability model partitions the pore space into two regions that have fast (fracture) and slow (matrix) rates of advective and dispersive transport of solutes. In contrast to previous work, we use the dual-permeability model herein to simulate the different colloid retention mechanisms that occur in fast (larger pore spaces; region 1) and slow (small pore spaces, dead end pores, and grain-to-grain contact points: region 2) velocity regions of homogeneous porous media. The dual-permeability model has not been previously used to gain insight into enhanced colloid retention processes in low-velocity regions of homogeneous porous media. The approach is somewhat analogous to multiphase flow and transport models that partition the pore space to regions accessible for the wetting (small pore spaces) and nonwetting (large pore spaces) phases. The small pore spaces in the dual-permeability model are assumed to maintain continuity by slow flow adjacent to the solid phase, in crevice sites near grain-to-grain contacts, and in small pores in the same way as the wetting phase in multiphase systems.

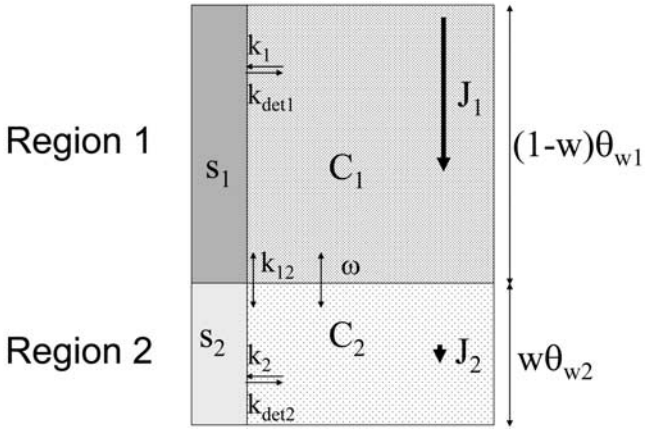

Figure 1. A conceptual picture of the flow and colloid transport processes that are simulated in the dual-permeability model. Model parameters are defined in the main text.

[15] Figure 1 presents a conceptual picture of the flow and colloid transport processes that are assumed to occur in the dual-permeability model. As indicated above, colloids that collide with solid surfaces in fast regions of the pore space experience different hydrodynamic forces than colloids in slow regions. The higher hydrodynamic forces in region 1 act to remove colloids from the solid surface in region 1, thus causing region 1 to be associated with lower rates of colloid retention. Colloid exchange in the aqueous phase may occur to and from ''slow'' water (region 2). In addition, in this work we also consider the potential for colloid exchange on the solid phase from fast to slow regions due to either rolling or sliding of colloids on the solid surface. The governing equations for water flow in the dual-permeability model are well known and are available in the literature [*Gerke and van Genuchten*, 1993a, 1993b; *Šimůnek and van Genuchten*, 2008]. The corresponding one-dimensional dual-permeability equations for local-scale colloid transport and retention are as follows:

$$\frac{\partial(\theta_{w1}C_1)}{\partial t} = -\frac{\partial J_1}{\partial z} + \frac{\Gamma_s}{1-w} - \theta_{w1}k_1C_1 + \rho_{b1}k_{\mathrm{det}\,1}s_1 \qquad (4)$$

$$\frac{\partial(\theta_{w2}C_2)}{\partial t} = -\frac{\partial J_2}{\partial z} - \frac{\Gamma_s}{w} - \theta_{w2}k_2C_2 + \rho_{b2}k_{\mathrm{det}2}s_2 \qquad (5)$$

$$\frac{\partial(\rho_{b1}s_1)}{\partial t} = \theta_{w1}k_1C_1 - \rho_{b1}k_{\mathrm{det}1}s_1 - \frac{\rho_{b1}k_{12}s_1}{1-w} \qquad (6)$$

$$\frac{\partial(\rho_{b2}s_2)}{\partial t} = \theta_{w2}k_2C_2 - \rho_{b2}k_{\mathrm{det}2}s_2 + \frac{\rho_{b1}k_{12}s_1}{w} \qquad (7)$$

$$\Gamma_s = \omega(1-w)\theta_{w1}(C_2 - C_1) \qquad (8)$$

where z [L] is distance, t [T] is time, C_1 and C_2 [N_c L^{-3}; N_c denotes the number of colloids] are the liquid phase concentrations of colloids in regions 1 and 2, s_1 and s_2 [N_c M^{-1}] are the solid phase concentrations of colloids in regions 1 and 2, θ_{w1} and θ_{w2} are the volumetric water contents in regions 1 and 2 [−], ρ_{b1} and ρ_{b2} are the bulk densities in regions 1 and 2 [M L^{-3}], k_1 and k_2 [T^{-1}] are the first-order colloid retention rate coefficients in regions 1 and 2, $k_{\mathrm{det}1}$ and $k_{\mathrm{det}2}$ [T^{-1}] are the first-order detachment coefficients in regions 1 and 2, J_1 and J_2 [N_c L^{-2} T^{-1}] are the total solute fluxes (sum of the advective and dispersive flux) for colloids in regions 1 and 2, ω [T^{-1}] is a coefficient for colloid exchange between liquids in regions 1 to 2, k_{12} [T^{-1}] is a coefficient for transfer of colloids from solid phase region 1 to 2, and w is the ratio of the volume of region 2 to the total volume (volume of region 1 plus volume of region 2). The term Γ_s [N L^{-3} T^{-1}] accounts for aqueous phase mass exchange of colloids between regions 1 and 2.

[16] Equations (4)–(8) were written in terms of local-scale mass balances of regions 1 and 2. To formulate the equations in terms of the total pore space, the mass balance equations for regions 1 and 2 need to be multiplied by (1-w) and w, respectively. The relationship between several variables at the local-scale and total pore space is provided below. Under steady state flow conditions, the total water flux (q_t; LT^{-1}) is defined as

$$q_t = (1-w)q_1 + wq_2 \qquad (9)$$

where q_1 (LT^{-1}) and q_2 (LT^{-1}) are the local-scale water fluxes in regions 1 and 2, respectively. Expressions for the total water content and bulk density are written in an analogous manner as equation (9). The total flux concentration of colloids (C_t, N_c L^{-3}) is given as [*Šimůnek and van Genuchten*, 2008]

$$C_t = \frac{wq_2C_2 + (1-w)q_1C_1}{wq_2 + (1-w)q_1} \qquad (10)$$

and the total solid phase colloid concentration (s_t, N_c M^{-1}) as

$$s_t = \frac{w\rho_{b2}s_2 + (1-w)\rho_{b1}s_1}{w\rho_{b2} + (1-w)\rho_{b1}} \qquad (11)$$

[17] The dual-permeability model outlined above has been implemented into the HYDRUS-1D computer model [*Šimůnek et al.*, 2007; *Šimůnek and van Genuchten*, 2008]. The code employs the Galerkin-type linear finite element method for spatial discretization of the governing differential equations, and a finite difference method to approximate temporal derivatives. A Crank-Nicholson finite difference scheme was used to solve the outlined transport equations sequentially (with equations for region 1 solved first). Complete details about the numerical techniques are provided in the HYDRUS-1D technical manual [*Šimůnek et al.*, 2007]. For the simulations discussed below, a third-type boundary condition was used at the inlet, and a concentration gradient of zero was fixed at z equal to the outlet depth. The initial concentration of the simulation domain was zero. We note that the HYDRUS-1D code allows model parameters to be fitted to the breakthrough curve and the retention profile simultaneously using a nonlinear least squares optimization routine based upon the Levenberg-Marquardt algorithm [*Marquardt*, 1963].

3.1. Model Parameters

[18] In this paper we apply the dual-permeability model to homogeneous porous media. Values of the volumetric water content and bulk density were therefore assumed to be the same for both regions 1 and 2, to be determined from independently measured values. Similarly, we assume that the dispersivity for both regions is equal and can be determined from conservative solute tracer data.

[19] Equations (1)–(3) indicate that colloid retention is "chemically and hydrodynamically" favorable in the smallest portions of the pore space (region 2). We therefore assume that k_2 can be determined from clean bed filtration theory [*Yao et al.*, 1971] as

$$k_2 = \frac{3(1-\theta_w)}{2d_{50}}\eta v \tag{12}$$

where v [L T^{-1}] is the average total pore water velocity, θ_w is the total volumetric water content [−], and d_{50} [L] is the median grain diameter. The parameter η is defined as the ratio of the integral of the colloid flux that strikes the collector to the rate at which particles flow toward the collector. This parameter was determined using the correlation expression of *Tufenkji and Elimelech* [2004]. Since colloid retention is favorable in region 2, the value of k_{det2} is set equal to zero.

[20] Colloid retention is assumed to be "chemically and hydrodynamically" unfavorable in the larger portions of the pore space defined by region 1. Two different conceptual approaches may be used to quantify colloid behavior in region 1. The first approach assumes that "irreversible" colloid retention occurs in region 1 (for given experimental conditions) as a result of chemical heterogeneity and surface roughness, or because of the potential for colloids to diffusion over the DLVO energy barrier [*Hubbe*, 1984; *Simoni et al.*, 1998; *Dong et al.*, 2002]. This "irreversible" colloid retention can be quantified with k_1 when k_{det1} is set equal to zero. The approach also implies that the influence of pore-scale hydrodynamics on colloid removal from the solid surface in region 1 has already occurred, in which case the value of k_{12} can be set equal to zero. The value of ω therefore reflects the lumped exchange of colloids from region 1 to 2 due to diffusion in the bulk solution and slow advection of weakly associated colloids (secondary minimum) near the solid phase. In this case, k_1 and ω can be determined by fitting to experimental data. We note here that *Gerke and van Genuchten* [1993b] presented an alternative model formulation for equation (8) to account for both diffusive and advective exchange between regions 1 and 2 under unsaturated conditions.

[21] The second approach considers all colloid retention to be "reversible" in region 1, while the value of k_1 is determined analogously to equation (12) ($k_1 = k_2$). With this assumption the values of k_{det1} and k_{12} are used to partition weakly associated colloids (secondary minimum) back to the aqueous phase or to the region 2 solid phase where they are "irreversibly" retained, respectively. In this case, the value of ω reflects diffusive exchange between regions 1 and 2. For advection dominated systems we assume that the value of ω goes to zero, and that the values of k_{det1} and k_{12} can be determined by fitting to experimental data.

[22] *Bradford et al.* [2006] presented an approach to estimate the advective water flux to the smallest regions of the pore space. In brief, the water flux in region 2 portions of the pore space can be calculated as

$$wq_2 = q_t \frac{k_{r2}}{k_{rw}} \tag{13}$$

where k_{rw} [−] is the water relative permeability and k_{r2} [−] is the water relative permeability to the low-velocity regions of the pore space. The value of k_{rw} is typically determined from capillary pressure data using a pore size distribution model. In analogy to this approach, the value of k_{r2} can be determined using the pore size distribution model of *Burdine* [1953] by limiting the integration to only region 2 areas of the porous medium as follows:

$$k_{r2}(S_w) = S_w^2 \frac{\int_0^{\gamma} R(S)^2 dS}{\int_0^1 R(S)^2 dS} = S_w^2\left[1-\left(1-\gamma^{1/m}\right)^m\right] \tag{14}$$

where S_w [−] is the water saturation in the porous medium, R [L] is pore radius distribution in the porous medium, S [−] is a dummy saturation variable of integration, and γ and m ($m = 1-2/n$) were defined in equation (3). When wq_2 and q_t are both known then it follows that $(1-w)q_1 = q_t - wq_2$. Furthermore, the value of w in the dual-permeability model is related to γ as

$$w = \frac{\gamma\varepsilon}{\theta_{w2}} \tag{15}$$

where ε[−] is the porosity of the porous medium. For saturated conditions the value of $\varepsilon = (1-w)\theta_{w1} + w\theta_{w2}$. If regions 1 and 2 have the same porosity, then $\varepsilon/\theta_{w2} = 1$ and hence $w = \gamma$.

[23] In summary, for steady state flow conditions in homogeneous porous media the dual-permeability model parameters can be measured independently or estimated from experimental data. Depending on the conceptual model choice, three critical model parameters were identified: k_1, ω, and wq_2; or k_{det1}, k_{12} and wq_2.

3.2. Example Simulations

[24] The sensitivity of dual-permeability model simulations to key parameters (ω, wq_2, q_t, and k_{12}) is explored in this section. All of the simulations were conducted for steady state water flow conditions. Breakthrough curves (at a depth of 10 cm) are plotted herein with the total relative flux concentrations on the y axis and pore volume on the x axis. The total relative flux concentration is defined as C_t/C_i where C_i [N$_c$ L^{-3}] is the colloid concentration of the influent tracer suspension. Final profiles of retained colloids are plotted herein with the total normalized solid phase colloid concentration (s_t/N_{ic}) on the x axis and dimensionless distance from the column inlet on the y axis, where N_{ic} [N$_c$] is the number of colloids in a unit volume of the influent colloid suspension. For these simulations values of the volumetric water content, bulk density, median grain

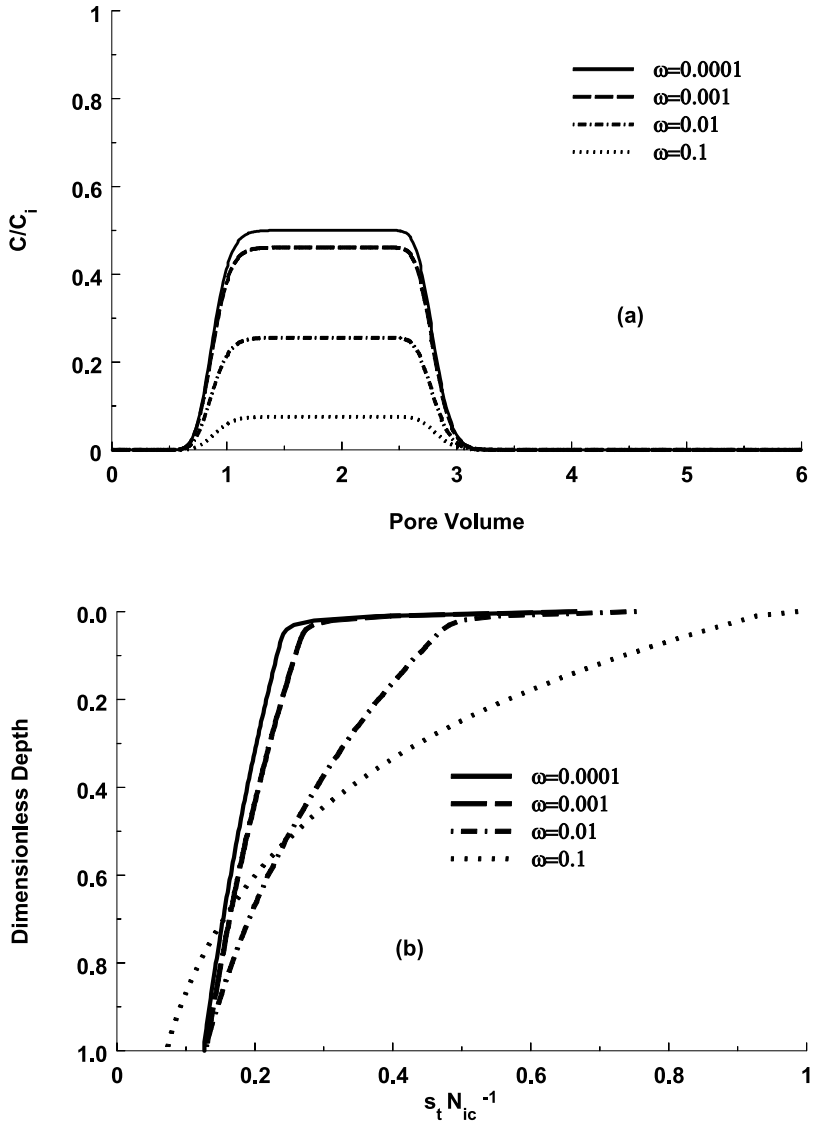

Figure 2. Plots of (a) simulated breakthrough curves and (b) retention profiles when wq_2 was 0.001 cm min^{-1}, q_t was 0.0918 cm min^{-1}, and ω was 0.0001, 0.001, 0.01, and 0.1 min^{-1}. Other model parameters are provided in the manuscript text.

size, and dispersivity were set equal to 0.334 cm^3 cm^{-3}, 1.765 g cm^3, 0.15 mm and 0.1 cm, respectively, to be consistent with sandy soils. The colloid input pulse duration was approximately two pore volumes. A summary of all model parameters that were employed in the simulations below is provided in the figure captions.

[25] Figure 2 presents plots of simulated breakthrough curves and retention profiles when wq_2 = 0.001 cm min^{-1}, q_t = 0.0918 cm min^{-1}, and ω was fixed at 0.0001, 0.001, 0.01, and 0.1 min^{-1}. The value of wq_2 in these simulations was selected to be less than 1% of q_t to reflect low flow to the smaller pore spaces as calculated by *Bradford et al.* [2006] for sandy soils. The value of k_1 was selected to be 3% of the favorable attachment condition rate (k_1 = 0.03*k_2) based on findings of *Dong et al.* [2002]. Notice that increasing ω produces lower effluent concentrations and greater amounts of colloid retention. The value of ω also has a pronounced effect on the shape of the colloid retention profile. When ω is large, colloid retention becomes consistent with the single region attachment/detachment model, in which case regions 1 and 2 are approaching a well mixed condition. In contrast, regions 1 and 2 are not well mixed when w is low. The overall colloid retention profile is then the sum of largely independent exponential profiles from regions 1 and 2. In this case, colloid retention occurs to a greater extent near the column inlet and produces an overall nonexponential retention profile because of the slower rate of advection and the high rate of retention in region 2.

[26] A sensitivity analysis was conducted to further investigate the influence of the water flux on colloid transport and retention. The water flux to low- and high-velocity regions is equal to wq_2 and $(1 - w)q_1$, respectively. Figure 3 presents plots of the simulated breakthrough curves and retention profiles when q_t was equal to 0.0918 cm min^{-1} and the value of wq_2 was taken to be 0, 0.001, 0.002, 0.004, and 0.008 cm min^{-1}. For reasons discussed above, the values wq_2 were selected to be low (<10% of q_t),

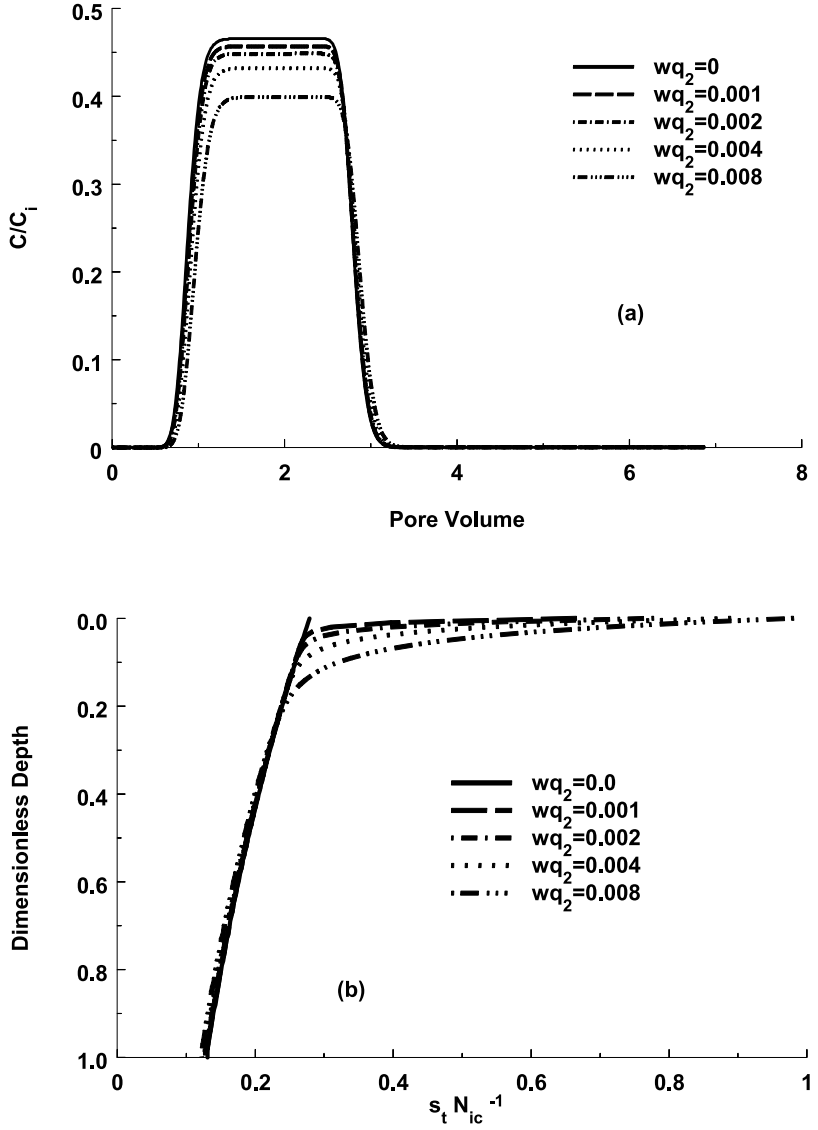

Figure 3. Plots of (a) simulated breakthrough curves and (b) retention profiles when q_t was equal to 0.0918 cm min^{-1} and the value of wq_2 was 0, 0.001, 0.002, 0.004, and 0.008 cm min^{-1}. Other model parameters are provided in the manuscript text.

while k_1 was set equal to $0.03*k_2$. The value of ω was selected to be 0.001 min^{-1} based on parameter sensitivity observed in Figure 2. Observe that changing the value of wq_2 had relatively little influence on the breakthrough curves, but a pronounced effect on the shape of the retention profiles (values of s_t/N_{ic} at a depth of 0.1 cm were 0.28, 0.40, 0.52, 0.68, and 0.83 g^{-1} when wq_2 was 0.0, 0.001, 0.002, 0.004, and 0.008 cm min^{-1}, respectively). In particular, higher values of wq_2 produced greater colloid retention at the column inlet that is not consistent with an exponential distribution with depth. As mentioned in the introduction, depth-dependent colloid retention profiles [*Bradford et al.*, 2003, 2006, 2007; *Tufenkji and Elimelech*, 2005; *Li and Johnson*, 2005] and earlier breakthrough times [*Ryan and Elimelech*, 1996; *Ginn*, 2002] have frequently been observed under unfavorable attachment conditions.

[27] Figure 4 presents plots of the simulated breakthrough curves and retention profiles when wq_2 was 0.001 cm $min^{-1}$and q_t was equal to 0.024, 0.046, 0.091, 0.181, and 0.361 cm min^{-1}. In these simulations values of wq_2, $k_1 = 0.03*k_2$, and $\omega = 0.001$ min^{-1} were selected based on justification provided earlier. Notice that higher values of q_t have a pronounced influence on the shape of the breakthrough curves and the retention profiles. Higher effluent concentrations occur with increasing q_t, while the shape of the retention profile becomes more uniform with depth. In particular observe that less colloid retention occurs at the column inlet with increasing q_t. This prediction is consistent with experimental observations that have shown decreasing colloid retention near the column inlet with increasing velocity [*Bradford et al.*, 2006, 2007]. We note here that classical filtration theory predicts that the retention profile will be exponential with distance regardless of the velocity.

[28] Increasing k_1 will also impact the breakthrough curves and retention profiles (data not shown). In particular, for increasing k_1 greater colloid retention will occur throughout the profile, leading to lower effluent concentrations. When k_1 and k_2 are equal and wq_2 is low then the

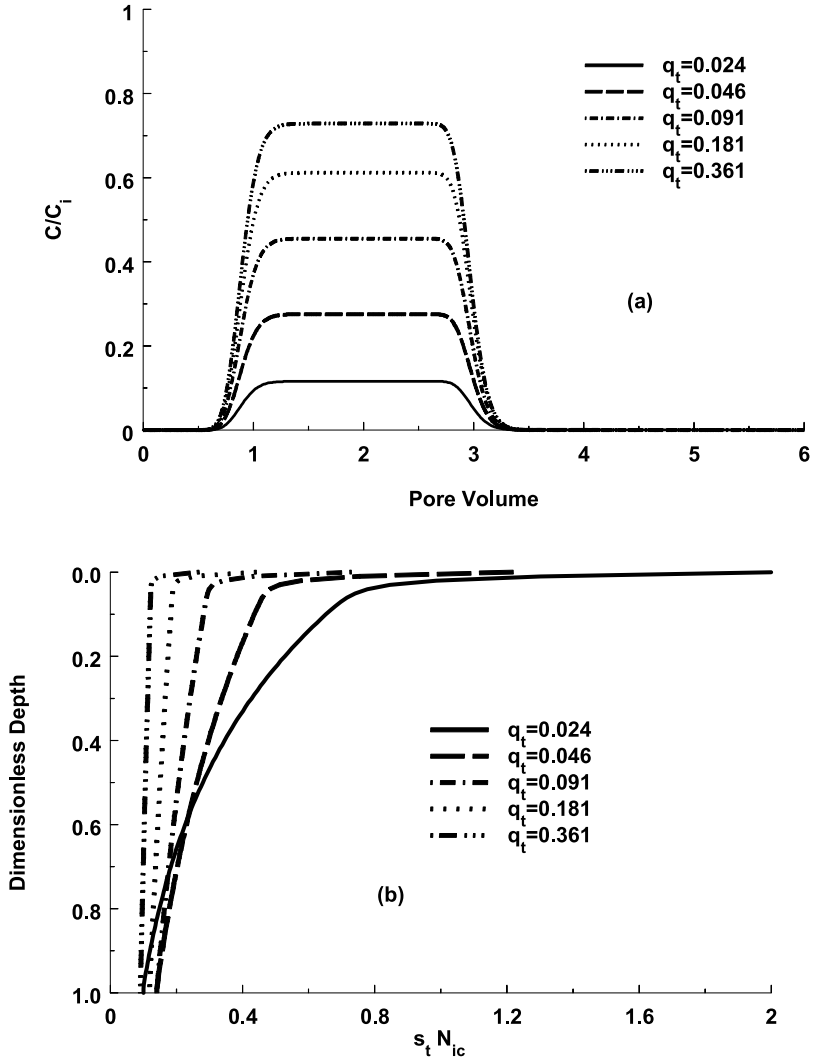

Figure 4. Plots of (a) the simulated breakthrough curves and (b) retention profiles when wq_2 was 0.001 cm min^{-1}and q_t was equal to 0.024, 0.046, 0.091, 0.181, and 0.361 cm min^{-1}. Other model parameters are provided in the manuscript text.

retention profile will approach results of a conventional single-region attachment/detachment model.

[29] When exchange of colloids on the solid phase (rolling) is considered in the model, then different values for k_1 and k_{det1} need to be employed to accurately reflect the effects of hydrodynamics on colloid retention. As discussed in section 3.1, when rolling occurs we assumed that k_1 is equal to k_2 to be consistent with an initially high rate of mass transfer to the solid-water interface. The values of k_{det1} and k_{12} are then used to partition colloids on the solid surface (region 1) back into solution (region 1) or to the solid phase in region 2, respectively. At equilibrium the value of $k_{det1} = k_1/(R-1)$, where R [−] is the retardation coefficient. For determination of k_{det1} we assumed a value of $R = 2.5$ to allow sufficient time for rolling to occur and this choice produces a slightly retarded breakthrough time for the colloids. Figure 5 shows plots of the simulated breakthrough curves and retention profiles when q_t = 0.0918 cm min^{-1}, wq_2 = 0.001 cm min^{-1}, and k_{12} was equal to 0.001, 0.01, 0.05, and 0.1 min^{-1}. Notice that the breakthrough curves and the retention profiles are sensitive to values of k_{12}. Little colloid retention occurs when k_{12} is small because of the low-mass transfer rate (rolling) to region 2, causing the colloids in region 1 to move back into the aqueous phase because of the high value of k_{det1}. Conversely, increasing k_{12} leads to lower effluent concentrations and greater colloid retention throughout the profile (effects are not localized to the column inlet).

3.3. Application to Data

[30] This section investigates the ability of the dual-permeability model to describe experimental colloid breakthrough curves and retention profiles that were presented by *Bradford et al.* [2007] for various solution chemistries (pH = 10 and ionic strength, IS), Darcy velocities, and colloid (carboxyl modified latex microspheres) and grain (Ottawa quartz sand) sizes. Table 1 provides a summary of the experimental conditions. DLVO calculations and batch experiments conducted for these same colloids, porous media, and solution chemistries indicated that conditions were highly unfavorable for colloid attachment [*Bradford*

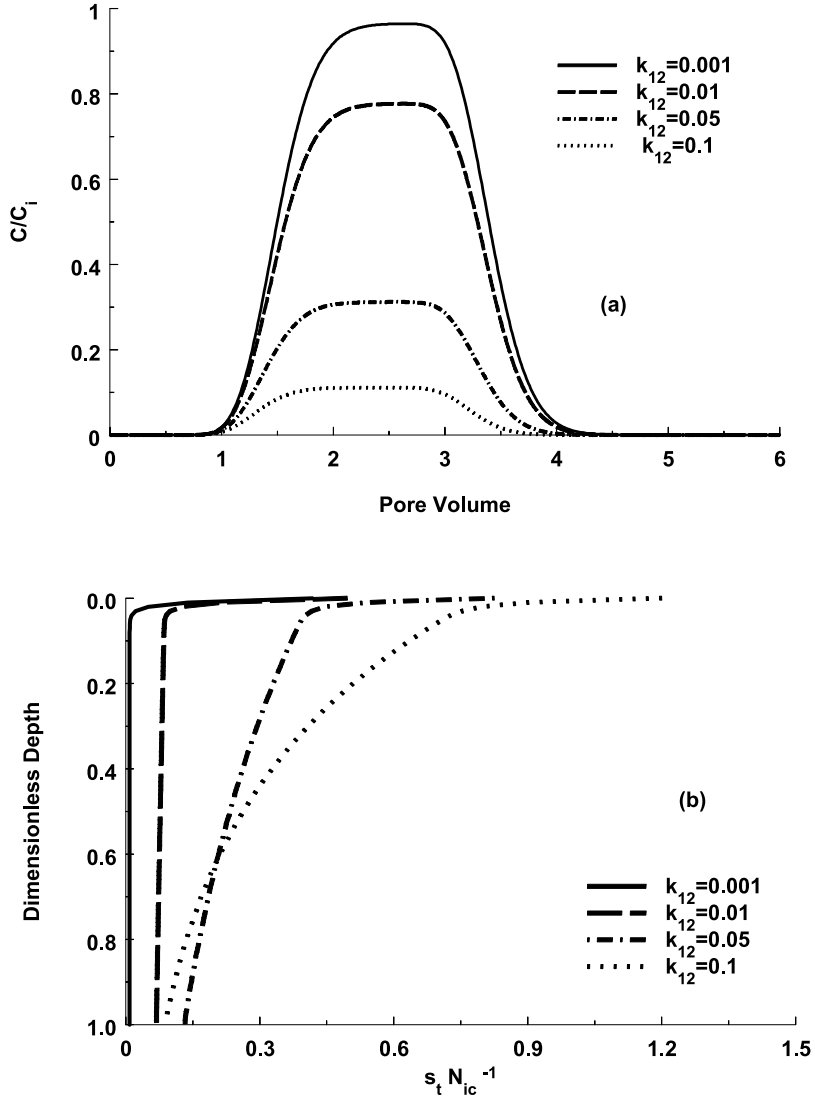

Figure 5. Plots of (a) the simulated breakthrough curves and (b) retention profiles when q_t was equal to 0.0918 cm min^{-1}, wq_2 was equal to 0.001 cm min^{-1}, and k_{12} was equal to 0.001, 0.01, 0.05, and 0.1 min^{-1}. Other model parameters are provided in the manuscript text.

Table 1. Summary of Experimental Conditions and Dual-Permeability Model Parameters[a]

d_c[b] (μm)	d_{50} (μm)	IS[c] (mM)	ε	q_t (cm min^{-1})	λ (cm)	wq_2/q_t	k_1 (min^{-1})	R^2_{BTC}	R^2_{RP}
3	360	6	0.35	0.096	0.718	0.011	0.008	0.974	0.989
3	240	6	0.32	0.104	0.280	0.004	0.042	0.976	0.997
3	150	6	0.35	0.096	0.718	0.008	0.058	0.936	0.998
1.1	150	56	0.35	0.099	0.393	0.008	0.040	0.940	0.995
1.1	150	56	0.36	0.446	0.393	0.001	0.061	0.980	0.934
1.1	150	6	0.33	0.104	0.393	0.015	0.001	0.977	0.947
1.1	150	31	0.35	0.098	0.393	0.011	0.003	0.961	0.876
1.1	150	56	0.35	0.099	0.393	0.008	0.040	0.940	0.995
1.1	150	81	0.35	0.084	0.393	0.005	0.037	0.980	0.992
1.1	150	106	0.34	0.101	0.393	0.013	0.202	-	0.998

[a]As used in the simulations presented in Figures 6–8, as well as the coefficient of linear regression for the goodness of the model fit to breakthrough curve (R^2_{BTC}) and retention profile (R^2_{RP}) data.
[b]Here is d_c colloid diameter.
[c]IS is ionic strength.

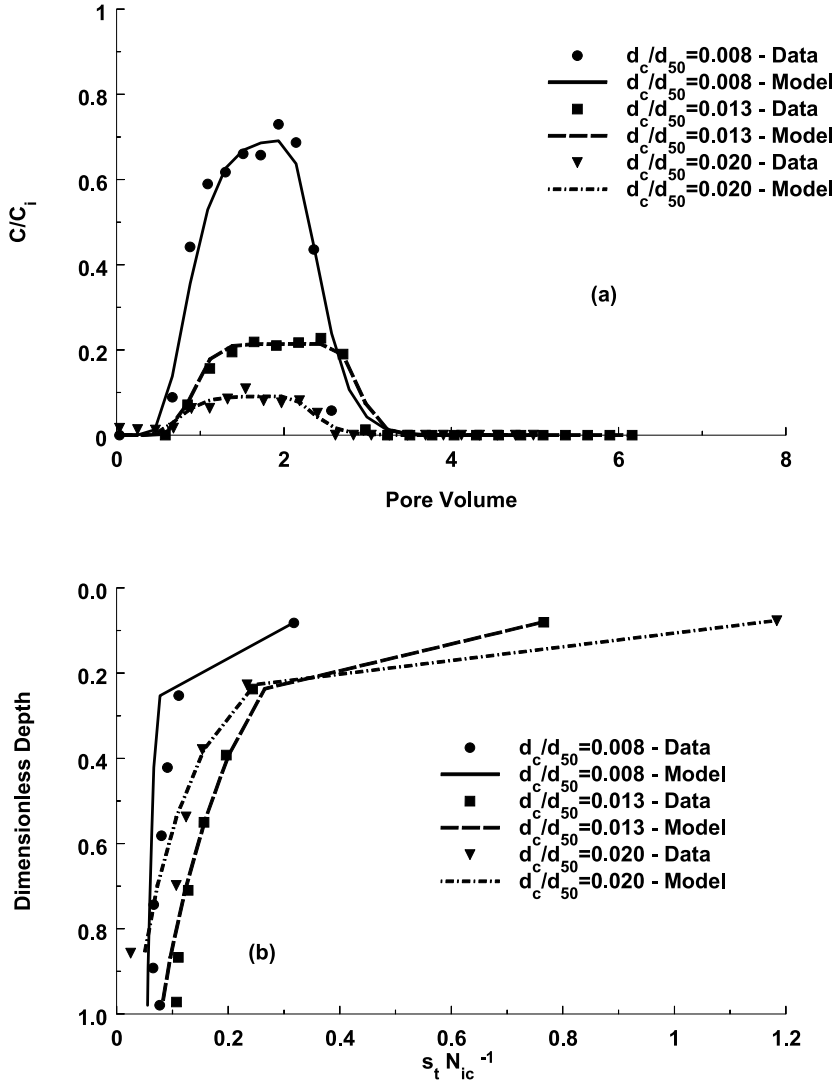

Figure 6. Plots of (a) observed and simulated breakthrough curves and (b) retention profiles for 3 mm colloids when q_t was approximately 0.1 cm min^{-1}, the solution ionic strength was 6 mM, the pH was 10, and d_{50} was equal to 360, 240, and 150 mm. Other model parameters are provided in the manuscript text and in Table 1.

et al., 2007]. In brief, colloid transport experiments were conducted by pumping a monodispersed colloid suspension upward through a vertically oriented saturated column (4.8 cm inside diameter and 13 cm in length) at a steady pore water velocity. After a given colloid tracer pulse duration was applied, a three-way valve was used to switch to eluting solution of the same solution chemistry for several more pore volumes. Effluent samples were collected and analyzed for colloid concentration using a Turner Quantech Fluorometer (Barnstead/Thermolyne, Dubuque, IA). Following completion of the colloid transport experiments, the spatial distribution of retained colloids in each packed column was determined by excavating the sand into tubes containing excess eluant solution, slowly shaking the tubes for 15 min, and measuring the concentration of the colloids in the excess solution with the fluorometer. A detailed discussion of the experimental conditions and protocols is given by *Bradford et al.* [2002, 2007].

[31] Dual-permeability model parameters were fitted to the colloid transport data discussed above. Information presented in section 3.2 was used to constrain the model fits. Figures 3 and 4 demonstrated that colloid retention near the inlet boundary can be controlled by the value of wq_2 that was associated with high rates of irreversible retention to region 2 when ω is low. Consistent with these conditions, the value of wq_2 was optimized with $\omega = 0.0001$ min^{-1} (see Figure 2), k_2 was determined from equation (12), and $k_{det2} = 0$. The value of $(1 - w)q_1$ was determined as $q_t - wq_2$. Figures 2–5 demonstrate that colloid retention away from the inlet boundary was controlled by k_1 or k_{12} depending on the conceptual model choice of "irreversible" or "reversible" retention in region 1, respectively. In the absence of additional information, we assumed "irreversible" colloid retention in region 1 by optimizing the value of k_1, and setting $k_{12} = 0$ and $k_{det1} = 0$. Other dual-permeability model parameters were determined from measured properties or were estimated. Values of the volumetric water content, bulk density, and dispersivity (λ; L) were assumed to be equal for both regions 1 and 2, and were set equal to measured values in the various sands. Table 1 provides a

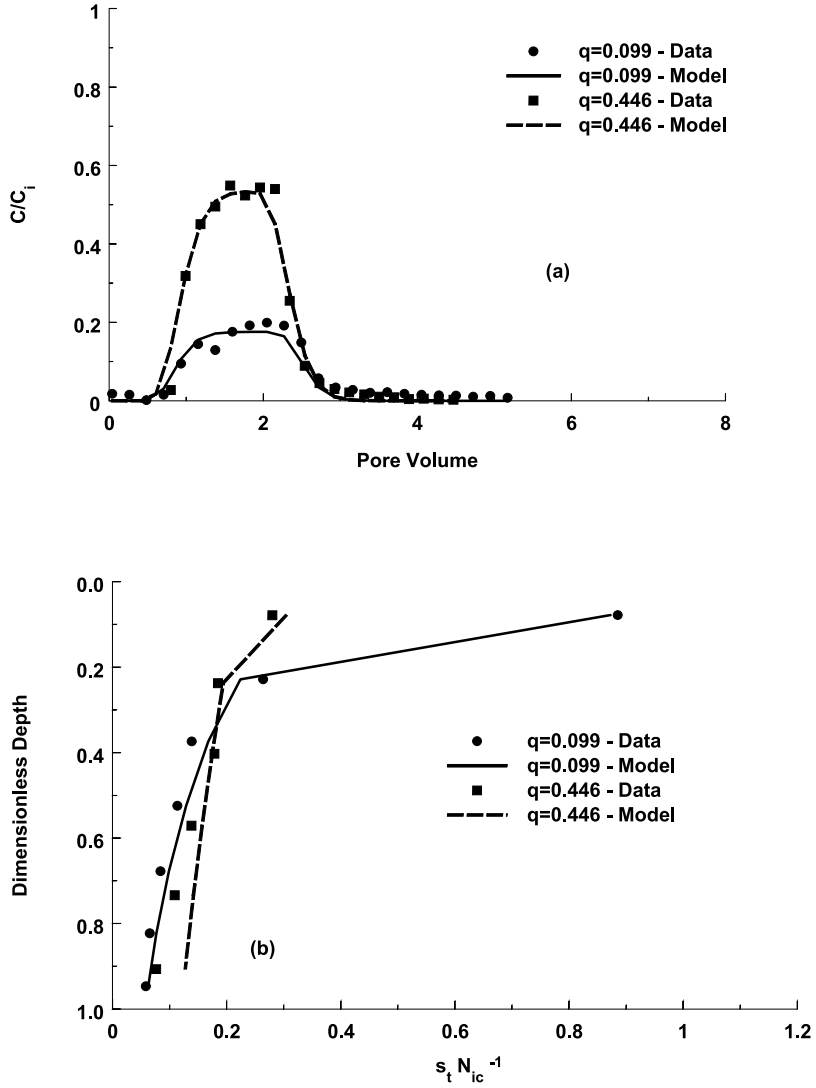

Figure 7. Plots of (a) observed and simulated breakthrough curves and (b) retention profiles for 1 μm colloids when the solution ionic strength was 56 mM, the pH was 10, d_{50} was 150 μm, and q_t was around 0.1 and 0.45 cm min^{-1}. Other model parameters are provided in the manuscript text and Table 1.

summary of dual-permeability model parameters that were used in the simulations discussed below, as well as the coefficient of linear regression for the goodness of the model fit to breakthrough curve (R^2_{BTC}) and retention profile (R^2_{RP}) data.

[32] Figure 6 presents plots of observed and simulated breakthrough curves (Figure 6a) and colloid retention profiles (Figure 6b) for 3 μm colloids when q_t was approximately 0.1 cm min^{-1}, the solution ionic strength was 6 mM, the pH was 10, and d_{50} was equal to 360, 240, and 150 μm. The dual-permeability model provided a good description of both the breakthrough curves ($R^2_{BTC} > 0.94$) and the retention profiles ($R^2_{RP} > 0.99$). The fitted value of wq_2 was low, less than 2% of q_t (Table 1). Hence, small amounts of flow to low velocity regions with enhanced rates of colloid retention provide one plausible explanation for nonexponential colloid retention profiles near the column inlet. Information presented by *Bradford et al.* [2006] indicates that for a given value of w the value of wq_2/q_t will depend on the grain size distribution, with more uniform sand having higher values of wq_2/q_t. Fitted values of wq_2/q_t in Table 1 are consistent with this prediction. Colloid retention in region 1 dominated the deposition profile shown in Figure 6b at dimensionless depths greater than around 0.2. Table 1 also indicates that k_1 increased with increasing d_{50}. This finding indicates that colloid retention in the higher-velocity regions of the pore space increased with increasing solid surface area, likely either due to attachment or colloid retention induced by surface roughness. We note that alternative conclusions may be reached if reversible colloid retention in region 1 is assumed (k_{12} and k_{det2} greater than zero).

[33] Figure 7 presents plots of observed and simulated breakthrough curves and colloid retention profiles for smaller 1 μm colloids when the solution ionic strength was 56 mM, the pH was 10, d_{50} was 150 μm, and q_t was around 0.1 and 0.45 cm min^{-1}. The dual-permeability model again provided a good description of the breakthrough curves and the colloid retention profiles. The

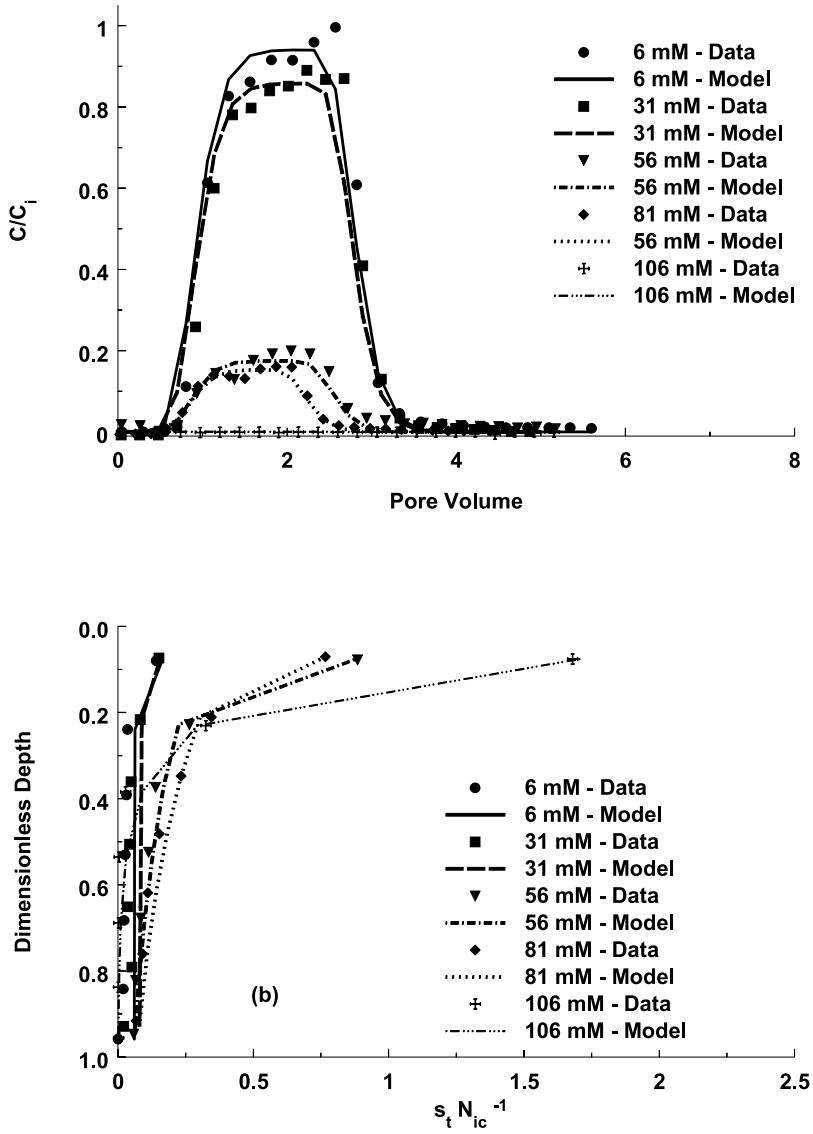

Figure 8. Plots of (a) observed and simulated breakthrough curves and (b) retention profiles for 1 μm colloids when d_{50} was 150 μm, q_t was 0.1 cm min^{-1}, the pH was 10, and the solution ionic strength was 6, 31, 56, 81, and 106 mM. Other model parameters are provided in the manuscript text and Table 1.

transport data for the higher water velocity system yielded a lower value of wq_2/q_t and a higher value of k_1. A lower value of wq_2/q_t with increasing velocity is expected based on equation (2) (the pressure gradient and the velocity are proportional to each other). An increase in k_1 with velocity is also expected based on filtration theory predictions. Hence, these observations both imply that the dual-permeability modeling approach accurately characterizes the physics of the system.

[34] Figure 8 shows plots of observed and simulated breakthrough curves and colloid retention profiles for 1 μm colloids when d_{50} was 150 μm, q_t was around 0.1 cm min^{-1}, the pH was 10, and the solution ionic strength was 6, 31, 56, 81, and 106 mM. The model provides a good description of the breakthrough curves and the colloid retention profiles. As the solution ionic strength increased the value of k_1 increased as expected because of greater attachment in the secondary minimum of the DLVO interaction energy profile. The value of wq_2, however, did not vary in a systematic fashion as predicted by equation (2). This is likely due to nonunique parameter fits and/or the assumed conceptual model of irreversible retention in region 1. In reality, it may be possible to have both reversible and irreversible colloid retention in region 1.

[35] For comparison purposes the data presented in Figures 6–8 were also simulated using the conventional first-order attachment-detachment model (single region) by optimizing the attachment (k_{att}, T^{-1}) and detachment (k_{det}, T^{-1}) coefficients. Table 2 provides a summary of fitted attachment-detachment model parameters, as well as R^2_{BTC} and R^2_{RP}. A comparison of Tables 1 and 2 reveals that the dual-permeability model provided superior fits to both breakthrough curves and especially the retention profiles when optimizing the same number of parameters. This finding suggests that the dual-permeability modeling approach provides a more physically realistic description of the physics of the system than the conventional attachment-detachment model. Another advantage of the

Table 2. Summary of Experimental Conditions and Attachment-Detachment Model Parameters[a]

d_c[b] (μm)	d_{50} (μm)	IS[c] (mM)	ε	q_t (cm min^{-1})	λ (cm)	k_{att} (min^{-1})	k_{det} (min^{-1})	R^2_{BTC}	R^2_{RP}
3	360	6	0.35	0.096	0.718	0.007	1.5E-4	0.956	0.610
3	240	6	0.32	0.104	0.280	0.042	5.7E-4	0.974	0.735
3	150	6	0.35	0.096	0.718	0.057	3.1E-6	0.917	0.773
1.1	150	56	0.35	0.099	0.393	0.039	3.0E-4	0.956	0.761
1.1	150	56	0.36	0.446	0.393	0.051	3.1E-5	0.981	0.948
1.1	150	6	0.33	0.104	0.393	0.002	2.2E-3	0.987	0.142
1.1	150	31	0.35	0.098	0.393	0.003	1.6E-3	0.982	0.471
1.1	150	56	0.35	0.099	0.393	0.039	3.0E-4	0.956	0.761
1.1	150	81	0.35	0.084	0.393	0.040	9.3E-6	0.973	0.999
1.1	150	106	0.34	0.101	0.393	0.285	9.9E-7	-	0.998

[a]As fitted to data shown in Figures 6–8, as well as the coefficient of linear regression for the goodness of the model fit to breakthrough curve (R^2_{BTC}) and retention profile (R^2_{RP}) data.
[b]Here is d_c colloid diameter.
[c]IS is ionic strength.

dual-permeability model is that specific hypotheses about the influence of hydrodynamics on colloid retention can be tested.

4. Summary and Conclusions

[36] Recent experimental and theoretical work has demonstrated that pore space geometry and hydrodynamics play an important role in colloid retention under unfavorable attachment conditions. In particular, hydrodynamic forces have been demonstrated to funnel weakly associated colloids to grain-to-grain contacts and to hydrodynamically isolated low-velocity (eddy) regions. A balance of adhesive and hydrodynamic torques acting on colloids in these locations indicated that enhanced retention will occur in these low-velocity regions. Consequently, conceptual models that consider the average pore water velocity in the porous medium and a single attachment rate coefficient are not always adequate to describe observed colloid retention profiles, which are frequently nonexponential with distance.

[37] In this work, we highlighted a model formulation that can be used to account for enhanced colloid retention in low-velocity regions of the pore space. The model conceptualized the pore domain in terms of low- and higher-velocity regions, and included provisions for advective and dispersive transport and first-order colloid retention and release in both regions. The model also considered colloid exchange between low- and higher-velocity regions of the pore space in the aqueous and solid (rolling) phases. On the basis of literature evidence, we assumed that enhanced colloid retention occurred in the low-velocity regions of the pore space. With this assumption, a sensitivity analysis was performed with the dual-permeability model parameters. Simulation results indicated that low amounts of advective transport to low-velocity regions of the pore space had a dramatic effect on the shape of the retention profile, especially near the inlet boundary. The total water flow rate was also shown to have a significant influence on the shape of the colloid retention profile near the inlet boundary. In this case, higher water velocities were found to produce less colloid retention near the inlet boundary because greater amounts of colloids bypassed the low-velocity regions. Both of these predictions are consistent with experimental observations that have been reported in the literature. Away from the inlet boundary, colloid retention was controlled by the deposition rate in the higher-velocity region, and the aqueous and solid phase exchange rates.

[38] Published colloid transport and retention data that were obtained for unfavorable attachment conditions for a range of colloid and sand sizes, water velocities, and solution chemistries were described using the dual-permeability model. Fitted model parameters exhibited systematic trends with grain size, velocity, and solution chemistry. The dual-permeability model provided a plausible interpretation for the experimental observations, and a reasonable approximation of the pore-scale physics controlling colloid retention under unfavorable attachment conditions.

[39] **Acknowledgments.** This research was supported by the 206 Manure and Byproduct Utilization Project of the USDA-ARS, by a grant from NRI (NRI 2006-02541), and by an interagency agreement with the EPA (IAG DW-12-92189901-0). Mention of trade names and company names in this manuscript does not imply any endorsement or preferential treatment by the USDA.

References

Abbaszadegan, M., M. W. LeChevallier, and C. P. Gerba (2003), Occurrence of viruses in US groundwaters, *J. Am. Water Works Assoc.*, *95*, 107–120.

Ahmadi, G., S. Guo, and X. Zhang (2007), Particle adhesion and detachment in turbulent flows including capillary forces, *Particulate Sci. Technol.*, *25*, 59–76, doi:10.1080/02726350601146432.

Bergendahl, J., and D. Grasso (1998), Colloid generation during batch leaching tests: Mechanics of disaggregation, *Colloids Surf. A*, *135*, 193–205, doi:10.1016/S0927-7757(97)00248-3.

Bergendahl, J., and D. Grasso (1999), Prediction of colloid detachment in a model porous media: Thermodynamics, *AIChE J.*, *45*, 475–484, doi:10.1002/aic.690450305.

Bergendahl, J., and D. Grasso (2000), Prediction of colloid detachment in a model porous media: Hydrodynamics, *Chem. Eng. Sci.*, *55*, 1523–1532, doi:10.1016/S0009-2509(99)00422-4.

Bradford, S. A., and S. Torkzaban (2008), Colloid transport and retention in unsaturated porous media: A review of interface-, collector-, and pore-scale processes and models, *Vadose Zone J.*, *7*, 667–681, doi:10.2136/vzj2007.0092.

Bradford, S. A., S. R. Yates, M. Bettahar, and J. Šimůnek (2002), Physical factors affecting the transport and fate of colloids in saturated porous media, *Water Resour. Res.*, *38*(12), 1327, doi:10.1029/2002WR001340.

Bradford, S. A., J. Šimůnek, M. Bettahar, M. T. van Genuchten, and S. R. Yates (2003), Modeling colloid attachment, straining, and exclusion in saturated porous media, *Environ. Sci. Technol.*, *37*, 2242–2250, doi:10.1021/es025899u.

Bradford, S. A., J. Šimůnek, M. Bettahar, Y. F. Tadassa, M. T. van Genuchten, and S. R. Yates (2005), Straining of colloids at textural interfaces, *Water Resour. Res.*, *41*, W10404, doi:10.1029/2004WR003675.

Bradford, S. A., J. Šimůnek, M. Bettahar, M. T. van Genuchten, and S. R. Yates (2006), Significance of straining in colloid deposition: Evidence and implications, *Water Resour. Res.*, *42*, W12S15, doi:10.1029/2005WR004791.

Bradford, S. A., S. Torkzaban, and S. L. Walker (2007), Coupling of physical and chemical mechanisms of colloid straining in saturated porous media, *Water Res.*, *41*, 3012–3024, doi:10.1016/j.watres.2007.03.030.

Burdine, N. T. (1953), Relative permeability calculations from pore size distribution data, *Trans. Am. Inst. Min. Metall. Pet. Eng.*, *198*, 71–78.

Chen, G., M. Flury, J. B. Harsh, and P. C. Lichtner (2005), Colloid-facilitated transport of cesium in variably saturated Hanford sediments, *Environ. Sci. Technol.*, *39*, 3435–3442, doi:10.1021/es048978+.

Cumbie, D. H., and L. D. McKay (1999), Influence of diameter on particle transport in a fractured shale saprolite, *J. Contam. Hydrol.*, *37*, 139–157, doi:10.1016/S0169-7722(98)00156-9.

Cushing, R. S., and D. F. Lawler (1998), Depth filtration: Fundamental investigation through three-dimensional trajectory analysis, *Environ. Sci. Technol.*, *32*, 3793–3801, doi:10.1021/es9707567.

Dane, J. H., and J. W. Hopmans (2002), Water retention and storage, in *Methods of Soil Analysis. Part 4, Physical Methods*, *Soil Sci. Soc. Am. Book Ser.*, vol. 5, edited by J. H. Dane and G. C. Topp, pp. 675–680, Soil Sci. Soc. Am., Madison, Wis.

Davis, A. M. J., and M. E. O'Neill (1977), Separation in a slow linear shear flow past a cylinder and a plane, *J. Fluid Mech.*, *81*, 551–564, doi:10.1017/S0022112077002225.

Davis, A. M. J., M. E. O'Neill, J. M. Dorrepaal, and K. B. Ranger (1976), Separation from the surface of two equal spheres in Stokes flow, *J. Fluid Mech.*, *77*, 625–644, doi:10.1017/S0022112076002814.

Derjaguin, B. V., and L. D. Landau (1941), Theory of the stability of strongly charged lyophobic sols and of the adhesion of strongly charged particles in solutions of electrolytes, *Acta Physicochim. URSS*, *14*, 733–762.

Dong, H., T. C. Onstott, C.-H. Ko, A. D. Hollingsworth, D. G. Brown, and B. J. Mailloux (2002), Theoretical prediction of collision efficiency between adhesion-deficient bacteria and sediment grain surface, *Colloids Surf. B*, *24*, 229–245, doi:10.1016/S0927-7765(01)00243-0.

Flint, L. E., and A. L. Flint (2002), Porosity, in *Methods Soil Analysis. Part 4, Physical Methods*, *Soil Sci. Soc. Am. Book Ser.*, vol. 5, edited by J. H. Dane and G. C. Topp, pp. 241–254, Soil Sci. Soc. Am., Madison, Wis.

Franchi, A., and C. R. O'Melia (2003), Effects of natural organic matter and solution chemistry on the deposition and reentrainment of colloids in porous media, *Environ. Sci. Technol.*, *37*, 1122–1129, doi:10.1021/es015566h.

Gaillard, J. F., C. Chen, S. H. Stonedahl, B. L. T. Lau, D. T. Keane, and A. I. Packman (2007), Imaging of colloidal deposits in granular porous media by X-ray difference micro-tomography, *Geophys. Res. Lett.*, *34*, L18404, doi:10.1029/2007GL030514.

Gerba, C. P., J. B. Rose, and C. N. Haas (1996), Sensitive populations: Who is at the greatest risk?, *Int. J. Food Microbiol.*, *30*, 113–123, doi:10.1016/0168-1605(96)00996-8.

Gerke, H. H. (2006), Preferential flow descriptions for structured soils, *J. Plant Nutrition Soil Sci.*, *169*, 382–400, doi:10.1002/jpln.200521955.

Gerke, H. H., and M. T. van Genuchten (1993a), A dual-porosity model for simulating the preferential movement of water and solutes in structured porous media, *Water Resour. Res.*, *29*, 305–319, doi:10.1029/92WR02339.

Gerke, H. H., and M. T. van Genuchten (1993b), Evaluation of a first-order water transfer term for variably saturated dual-porosity flow models, *Water Resour. Res.*, *29*, 1225–1238, doi:10.1029/92WR02467.

Ginn, T. R. (2002), A travel time approach to exclusion on transport in porous media, *Water Resour. Res.*, *38*(4), 1041, doi:10.1029/2001WR000865.

Goldman, A. J., R. G. Cox, and H. Brenner (1967), Slow viscous motion of a sphere parallel to a plane wall—I motion through a quiescent fluid, *Chem. Eng. Sci.*, *22*, 637–651, doi:10.1016/0009-2509(67)80047-2.

Grolimund, D., and M. Borkovec (2001), Release and transport of colloidal particles in natural porous media: 1. Modeling, *Water Resour. Res.*, *37*, 559–570, doi:10.1029/2000WR900285.

Grolimund, D., M. Borkovec, K. Barmettler, and H. Sticher (1996), Colloid-facilitated transport of strongly sorbing contaminants in natural porous media: A laboratory column study, *Environ. Sci. Technol.*, *30*, 3118–3123, doi:10.1021/es960246x.

Hahn, M. W., and C. R. O'Melia (2004), Deposition and reentrainment of Brownian particles in porous media under unfavorable chemical conditions: Some concepts and applications, *Environ. Sci. Technol.*, *38*, 210–220, doi:10.1021/es030416n.

Hahn, M. W., D. Abadzic, and C. R. O'Melia (2004), Aquasols: On the role of secondary minima, *Environ. Sci. Technol.*, *38*, 5915–5924, doi:10.1021/es049746d.

Harvey, R. W., and S. P. Garabedian (1991), Use of colloid filtration theory in modeling movement of bacteria through a contaminated sandy aquifer, *Environ. Sci. Technol.*, *25*, 178–185, doi:10.1021/es00013a021.

Herzig, J. P., D. M. Leclerc, and P. L. Goff (1970), Flow of suspensions through porous media: Application to deep filtration, *Ind. Eng. Chem.*, *62*, 8–35, doi:10.1021/ie50725a003.

Hill, W. A. (1957), An analysis of sand filtration, *J. Sanitary Eng. Div. Am. Soc. Civ. Am.*, *83*(SA3), 1276–1279.

Hubbe, M. A. (1984), Theory of detachment of colloidal particles from plat surfaces exposed to flow, *Colloids Surf.*, *12*, 151–178, doi:10.1016/0166-6622(84)80096-7.

Johnson, K. L., K. Kendall, and A. D. Roberts (1971), Surface energy and the contact of elastic solids, *Proc. R. Soc. London, Ser. A*, *324*, 301–313, doi:10.1098/rspa.1971.0141.

Johnson, W. P., X. Li, and S. Assemi (2007a), Deposition and re-entrainment dynamics of microbes and non-biological colloids during non-perturbed transport in porous media in the presence of an energy barrier to deposition, *Adv. Water Resour.*, *30*, 1432–1454, doi:10.1016/j.advwatres.2006.05.020.

Johnson, W. P., X. Li, and G. Yal (2007b), Colloid retention in porous media: Mechanistic confirmation of wedging and retention in zones of flow stagnation, *Environ. Sci. Technol.*, *41*, 1279–1287, doi:10.1021/es061301x.

Khilar, K. C., and H. S. Fogler (1998), *Migration of Fines in Porous Media*, Kluwer Acad., Dordrecht, Netherlands.

Kim, S. B., M. Y. Corapcioglu, and D. J. Kim (2003), Effect of dissolved organic matter and bacteria on contaminant transport in riverbank filtration, *J. Contam. Hydrol.*, *66*, 1–23, doi:10.1016/S0169-7722(03)00025-1.

Kuznar, Z. A., and M. Elimelech (2007), Direct microscopic observation of particle deposition in porous media: Role of the secondary energy minimum, *Colloids Surf. A*, *294*, 156–162, doi:10.1016/j.colsurfa.2006.08.007.

Li, X., and W. P. Johnson (2005), Non-monotonic variations in removal rate coefficients of microspheres in porous media under unfavorable deposition conditions, *Environ. Sci. Technol.*, *39*, 1658–1665, doi:10.1021/es048963b.

Li, X., P. Zhang, C. L. Lin, and W. P. Johnson (2005), Role of hydrodynamic drag on microsphere deposition and re-entrainment in porous media under unfavorable conditions, *Environ. Sci. Technol.*, *39*, 4012–4020, doi:10.1021/es048814t.

Li, X., C.-L. Lin, J. D. Miller, and W. P. Johnson (2006), Pore-scale observation of microsphere deposition at grain-to-grain contacts over assemblage-scale porous media domains using X-ray microtomography, *Environ. Sci. Technol.*, *40*, 3762–3768, doi:10.1021/es0525004.

Logan, B. E., D. G. Jewett, R. G. Arnold, E. J. Bouwer, and C. R. O'Melia (1995), Clarification of clean-bed filtration models, *J. Environ. Eng.*, *121*, 869–873, doi:10.1061/(ASCE)0733-9372(1995)121:12(869).

Loge, F. J., D. E. Thompson, and R. C. Douglas (2002), PCR detection of specific pathogens in water: A risk-based analysis, *Environ. Sci. Technol.*, *36*, 2754–2759, doi:10.1021/es015777m.

Marquardt, D. W. (1963), An algorithm for least squares estimation of nonlinear parameters, *SIAM J. Appl. Math.*, *11*, 431–441.

Mays, D. C., and J. R. Hunt (2005), Hydrodynamic aspects of particle clogging in porous media, *Environ. Sci. Technol.*, *39*, 577–584, doi:10.1021/es049367k.

McDowell-Boyer, L. M., J. R. Hunt, and N. Sitar (1986), Particle transport through porous media, *Water Resour. Res.*, *22*, 1901–1921, doi:10.1029/WR022i013p01901.

Mishra, S., J. Jeevan, C. K. Ramesh, and L. Banwari (2001), In situ bioremediation potential of an oily sludge-degrading bacterial consortium, *Curr. Microbiol.*, *43*, 328–335, doi:10.1007/s002840010311.

Nelson, K. E., and T. R. Ginn (2005), Colloid filtration theory and the Happel sphere-in-cell model revisited with direct numerical simulation, *Langmuir*, *21*, 2173–2184, doi:10.1021/la048404i.

O'Neill, M. N. (1968), A sphere in contact with a plane wall in a slow linear shear flow, *Chem. Eng. Sci.*, *23*, 1293–1298, doi:10.1016/0009-2509(68)89039-6.

Padilla, I. Y., T. C. Jim Yeh, and M. H. Conklin (1999), The effect of water content on solute transport in unsaturated porous media, *Water Resour. Res.*, *35*, 3303–3313, doi:10.1029/1999WR900171.

Rajagopalan, R., and C. Tien (1976), Trajectory analysis of deep-bed filtration with the sphere-in-cell porous-media model, *AIChE J.*, *22*, 523–533, doi:10.1002/aic.690220316.

Redman, J. A., S. L. Walker, and M. Elimelech (2004), Bacterial adhesion and transport in porous media: Role of the secondary energy minimum, *Environ. Sci. Technol.*, *38*, 1777–1785, doi:10.1021/es034887l.

Ryan, J. N., and M. Elimelech (1996), Colloid mobilization and transport in groundwater, *Colloids Surf. A*, *107*, 1–56, doi:10.1016/0927-7757(95)03384-X.

Sharma, M. M., H. Chamoun, D. S. H. Sita Rama Sarma, and R. S. Schechter (1992), Factors controlling the hydrodynamic detachment of particles from surfaces, *J. Colloid Interface Sci.*, *149*, 121–134, doi:10.1016/0021-9797(92)90398-6.

Sheng, P., and M. Zhou (1992), Immiscible-fluid displacement: Contact-line dynamics and the velocity-dependent capillary pressure, *Phys. Rev. A*, *45*, 5694–5708, doi:10.1103/PhysRevA.45.5694.

Simoni, S. F., H. Harms, T. N. P. Bosma, and A. J. B. Zehnder (1998), Population heterogeneity affects transport of bacteria through sand columns at low flow rates, *Environ. Sci. Technol.*, *32*, 2100–2105, doi:10.1021/es970936g.

Šimůnek, J., and M. T. van Genuchten (2008), Modeling nonequilibrium flow and transport using HYDRUS, *Vadose Zone J.*, *7*, 782–797, doi:10.2136/vzj2007.0074.

Šimůnek, J., N. J. Jarvis, M. T. van Genuchten, and A. Gärdenäs (2003), Review and comparison of models for describing non-equilibrium and preferential flow and transport in the vadose zone, *J. Hydrol.*, *272*, 14–35, doi:10.1016/S0022-1694(02)00252-4.

Šimůnek, J., C. He, L. Pang, and S. A. Bradford (2006), Colloid-facilitated transport in variably saturated porous media: Numerical model and experimental verification, *Vadose Zone J.*, *5*, 1035–1047, doi:10.2136/vzj2005.0151.

Šimůnek, J., M. T. van Genuchten, and M. Šejna (2007), The HYDRUS-1D software package for simulating the one-dimensional movement of water, heat, and multiple solutes in variably saturated media, version 4.0, *HYDRUS Software Ser. 3*, 315 pp., Dep. of Environ. Sci., Univ. of Calif., Riverside.

Soltani, M., and G. Ahmadi (1994), On particle adhesion and removal mechanics in turbulent flows, *J. Adhesion Sci. Technol.*, *8*, 763–785, doi:10.1163/156856194X00799.

Taneda, S. (1979), Visualization of separating Stokes flows, *J. Phys. Soc. Jpn.*, *46*, 1935–1942, doi:10.1143/JPSJ.46.1935.

Tong, M., X. Li, C. N. Brow, and W. P. Johnson (2005), Detachment-influenced transport of an adhesion-deficient bacterial strain within water-reactive porous media, *Environ. Sci. Technol.*, *39*, 2500–2508, doi:10.1021/es049013t.

Toride, N., M. Inoue, and F. J. Leij (2003), Hydrodynamic dispersion in an unsaturated dune sand, *Soil Sci. Soc. Am. J.*, *67*, 703–712.

Torkzaban, S., S. A. Bradford, and S. L. Walker (2007), Resolving the coupled effects of hydrodynamics and DLVO forces on colloid attachment to porous media, *Langmuir*, *23*, 9652–9660, doi:10.1021/la700995e.

Torkzaban, S., S. A. Bradford, and S. L. Walker (2008a), Colloid transport in unsaturated porous media: The role of water content and ionic strength on particle straining, *J. Contam. Hydrol.*, *96*, 113–127, doi:10.1016/j.jconhyd.2007.10.006.

Torkzaban, S., S. S. Tazehkand, S. L. Walker, and S. A. Bradford (2008b), Transport and fate of bacteria in porous media: Coupled effects of chemical conditions and pore space geometry, *Water Resour. Res.*, *44*, W04403, doi:10.1029/2007WR006541.

Tsai, C. J., D. Y. H. Pui, and B. Y. H. Liu (1991), Particle detachment from disk surfaces of computer disk drives, *J. Aerosol Sci.*, *22*, 737–746, doi:10.1016/0021-8502(91)90066-Q.

Tufenkji, N., and M. Elimelech (2004), Correlation equation for predicting single-collector efficiency in physiochemical filtration in saturated porous media, *Environ. Sci. Technol.*, *38*, 529–536, doi:10.1021/es034049r.

Tufenkji, N., and M. Elimelech (2005), Breakdown of colloid filtration theory: Role of the secondary energy minimum and surface charge heterogeneities, *Langmuir*, *21*, 841–852, doi:10.1021/la048102g.

Tufenkji, N., J. A. Redman, and M. Elimelech (2003), Interpreting deposition patterns of microbial particles in laboratory-scale column experiments, *Environ. Sci. Technol.*, *37*, 616–623.

van Genuchten, M. T. (1980), A closed-form equation for predicting the hydraulic conductivity of unsaturated soils, *Soil Sci. Soc. Am. J.*, *44*, 892–898.

Verwey, E. J. W., and J. T. G. Overbeek (1948), *Theory of the Stability of Lyophobic Colloids*, Elsevier, Amsterdam.

Vidali, M. (2001), Bioremediation: An overview, *Pure Appl. Chem.*, *73*, 1163–1172, doi:10.1351/pac200173071163.

Xu, S., B. Gao, and J. E. Saiers (2006), Straining of colloidal particles in saturated porous media, *Water Resour. Res.*, *42*, W12S16, doi:10.1029/2006WR004948.

Yao, K. M., M. T. Habibian, and C. R. O'Melia (1971), Water and waste water filtration: Concepts and applications, *Environ. Sci. Technol.*, *5*, 1105–1112, doi:10.1021/es60058a005.

Yoon, J. S., J. T. Germaine, and P. J. Culligan (2006), Visualization of particle behavior with a porous medium: Mechanisms for particle filtration and retardation during downward transport, *Water Resour. Res.*, *42*, W06417, doi:10.1029/2004WR003660.

S. A. Bradford, US Salinity Laboratory, ARS, USDA, 450 West Big Springs Road, Riverside, CA 92507, USA. (scott.bradford@ars.usda.gov)

F. Leij, 43 Tortuga Cay, Aliso Viejo, CA 92656, USA.

J. Šimůnek and S. Torkzaban, Department of Environmental Science, University of California, Riverside, CA 92521, USA.

M. T. van Genuchten, Department of Mechanical Engineering, Federal University of Rio de Janeiro, Rio de Janeiro, RJ CEP 21945-970, Brazil.